



OPEN

Covert thermal barcodes based on phase change nanoparticles

SUBJECT AREAS:
NANOSCIENCE AND
TECHNOLOGY
MATERIALS SCIENCE

Binh Duong, Helin Liu, Liyuan Ma & Ming Su

Department of Biomedical Engineering, Worcester Polytechnic Institute, MA 01609.

Received
10 April 2014

Accepted
14 May 2014

Published
5 June 2014

Correspondence and
requests for materials
should be addressed to
M.S. (msu2@wpi.edu)

An unmet need is to develop covert barcodes that can be used to track-trace objects, and authenticate documents. This paper describes a new nanoparticle-based covert barcode system, in which a selected panel of solid-to-liquid phase change nanoparticles with discrete and sharp melting peaks is added in a variety of objects such as explosive derivative, drug, polymer, and ink. This method has high labeling capacity owing to the small sizes of nanoparticles, sharp melting peaks, and large scan range of thermal analysis. The thermal barcode can enhance forensic investigation by its technical readiness, structural covertness, and robustness.

Barcodes such as Universal Product Codes (UPC) are ubiquitously used to tag trading objects, but the visible barcodes can be altered or duplicated, facing increasing challenges such as product counterfeiting and unlawful use of objects¹. To protect product authentication, covert (invisible) taggants can be added in objects of interest (explosive, drug formulation, paper or ink) during manufacturing processes so that each object has its own code for tracking purposes^{2,3}. Forensic investigation can thus be efficiently enhanced by tracing a specific object to its manufacturer, vendor or purchaser. However, molecular or chemical taggants are not suitable for serialization due to small coding space⁴; fluorescent taggants are limited by availability of materials with minimal spectral overlap⁵; glass/plastic micro-spheres and fibers are often used as taggants, but have low coding capacity^{6,7}; graphical coding achieved by a lithographical technique is limited by structural integrity, material choice, and imaging identification^{8,9}; DNA barcodes offer high coding capacity, but they can be degraded at ambient condition and require polymerase chain reaction amplification for readout¹⁰.

Small sized nanoparticles have potentials as covert barcodes, but the lack of nanoparticle-specific physical property restricts their ability to label each object in a series. Briefly, there is no particle-specific magnetic or electrochemical property, meaning that one type of nanoparticle cannot be distinguished from others based on their magnetic or electro-chemical properties. Semiconducting or metallic nanoparticles have broad fluorescent or plasmonic emission peaks (peak width at half height of 150 nm), which limits the type of optically distinguishable nanoparticles between 400–900 nm to only a few¹¹. Plasmonic nanoparticle enhanced Raman scattering has sharp peaks over a large wavelength range, but available Raman active dyes are limited and quantitative signals are hard to obtain¹². Metallic nanorods containing alternating layers of metals require a high resolution optical microscope to detect optical contrast between adjacent segments¹³.

This article describes a new high capacity covert barcode system, in which a panel of solid-to-liquid phase change nanoparticles is added into an object and used as thermal barcode to tag drugs and explosives. The melting temperature of each type of nanoparticles is derived using differential scanning calorimetry (DSC). In order to avoid size dependent melting temperature reduction, nanoparticles are synthesized with diameter larger than the thermodynamic critical diameter (~ 20 nm)¹⁴. In order to achieve high coding capacity, pure substances and their eutectic mixtures can be used to make nanoparticles, where sharp melting peaks exist over a large temperature range during a linear thermal scan with DSC¹⁵. Since the eutectic mixtures go directly from solid phase to liquid phase without pasty stage, sharp melting peaks similar to those of pure substances can be obtained¹⁶. According to the combination law of phase diagram, ten different metals that can form one binary eutectic alloy among any two of them can form 45 types of binary alloys, 120 types of ternary eutectic alloys, 210 types of quaternary eutectic alloys, and so on. The total number of pure metals and eutectic alloys (with sharp melting peak) will reach 1,023, which can be derived graphically from Pascal's triangle using

$$\sum_{k=1}^n C_n^k - 1 \approx \sum_{k=1}^n \frac{n!}{k!(n-k)!} - 1 = 2^n - 1 \quad (1)$$

where n is the total number of metals, and k is the number of metals in one nanoparticle. Note that the combination corresponding to no metal (where n is 0) should be removed.



Results & Discussion

Ten different metals that can form at least one binary eutectic alloys among any two of them have been identified, including aluminum, bismuth, cadmium, copper, gadolinium, indium, lead, magnesium, palladium and silver. The eutectic compositions and corresponding melting temperatures can be derived by using the Calculation of Phase Diagram (Pandat 8.1 software), in which total Gibbs free energy is calculated as a function of the atomic ratio of the elements in a system¹⁷. At any given temperature, pressure and composition, Gibbs free energy is the lowest when all phases reach thermodynamic equilibrium. The latent heat of a eutectic alloy is calculated from the latent heats of the elements and their atomic ratio. Figure 1A shows the calculated phase diagram of lead-tin alloy with a eutectic composition of 38% and temperature of 183°C, which are close to the measured value of 37% and 184.5°C for lead-tin nanoparticles (Figure 1A inset). The transmission electron microscopy (TEM) image and X-ray fluorescence (XRF) spectrum of lead-tin nanoparticles can be found in the supporting information (SI, Figure S1). The calculated and measured melting temperatures of ten metals and alloys are close to each other (Figure 1B), where all data points are on a line with slope of 45°. Figure 1C shows the relation between calculated and measured latent heats of fusion of metals and alloys. Some calculated latent heats of fusion are lower than the measured ones, which is due to the partial oxidization of the nanoparticles. This is supported by the fact that metals and alloys with lower melting points are easily oxidized. Figure 1D plots the calculated melting temperatures and the latent heats of fusion of 53 types of metals and eutectic alloys. If these nanoparticles are used to form barcodes, the total combination will reach $2^{50}-1$, or 10^{15} .

Nanoparticles of four metals (bismuth, indium, tin and lead) and their selected eutectic alloys (binary, ternary and quaternary eutectic alloys) are used to tag dinitrotoluene (DNT), which is a trinitrotoluene (TNT) simulator. To prevent explosion while mixing metals/alloys with explosive materials, the nanoparticles are encapsulated inside silica shells. Figure 2A shows a scanning electron microscopy (SEM) image of silica encapsulated indium-tin alloy nanoparticles.

The average diameter of the nanoparticles (200 nm) is larger than the critical size, thus their melting temperatures are the same as the bulk counterpart (Figure 2A inset). X-ray fluorescence (XRF) analysis confirms the presence of indium (22.8 and 25.6 keV) and tin (23.8 and 26.7 keV) in eutectic alloy nanoparticles (Figure S2). Nanoparticles are mixed with DNT powder at a mass ratio of 1 to 100 (nanoparticle to DNT). DNT color (yellowish) does not change at this mass ratio. In one case, the DNT-nanoparticle mixture is dissolved in ethanol, and nanoparticles are collected by centrifugation prior to DSC testing. The melting temperature (120°C) is the same as that shown in Figure 2A inset, confirming the existence of the nanoparticles in the mixture. In another case, the DNT-nanoparticle mixture is ignited inside a container, and the debris is collected by rinsing the container, followed by centrifugation. Figure 2B shows the melting peaks of 12 types of nanoparticles (indium, tin, bismuth, lead, zinc and their eutectic alloys) collected from the debris, suggesting this method can be used to track-trace explosives after detonation. Four types of nanoparticles (indium, tin, bismuth, and indium-tin-bismuth eutectic alloy) have been used to form 15 different thermal barcodes, which are added into different batches of DNT powder. Figure 2C shows DSC curves of barcodes detected in DNT.

Phase change nanoparticles can be used for drug authentication. Nanoparticles of organic solids, i.e., stearic acid, palmitic acid, paraffin wax ($C_{18}H_{38}$) and polyethylene, have been made using water-in-oil emulsion reactions. In order to prevent agglomeration, these nanoparticles are encapsulated inside polystyrene shells. Figure 3A is a TEM image of encapsulated paraffin nanoparticles with melting point of 28°C (Figure 3A inset). Dynamic light scattering data shows an average nanoparticle diameter of 200 nm (Figure S3A). Fourier transform infrared spectroscopy (FTIR) spectra confirm the composition of the nanoparticles (Figure S3B). To demonstrate the feasibility of making eutectic organic solids, the melting temperatures of a mixture of palmitic acid (59°C) and stearic acid (68°C) at different mass ratios is calculated as shown in Figure 3B. The calculated eutectic melting temperature (52°C) is close to the experimentally measured one (54°C) (Figure 3B inset). A selected panel of organic

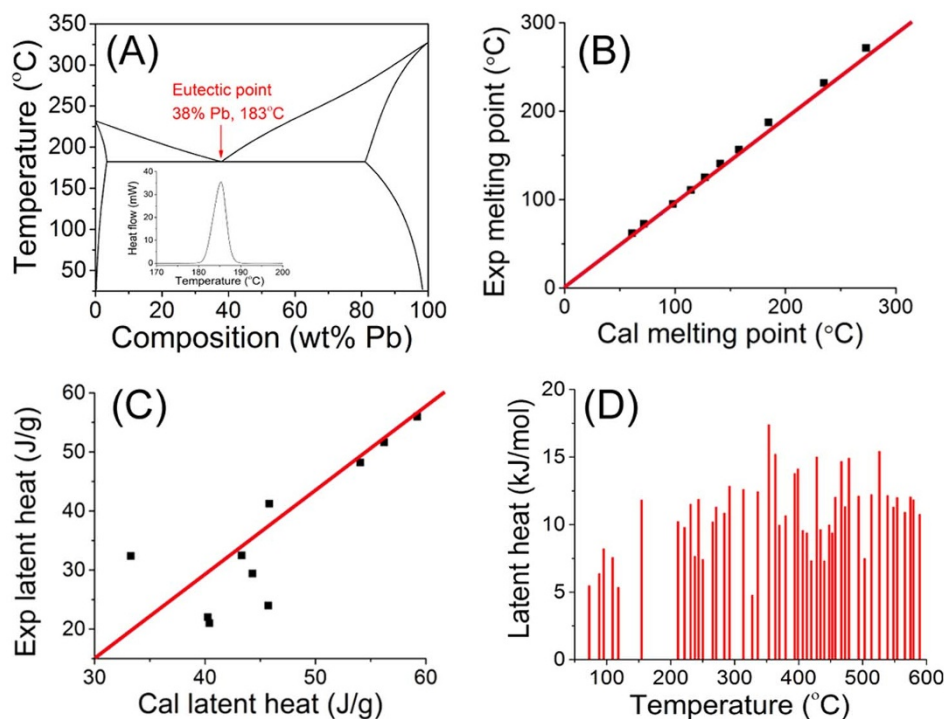


Figure 1 | (A) Calculated lead-tin phase diagram and DSC curve of their eutectic alloy (inset). The calculated melting points (B) and latent heats of fusion (C) of metals and eutectic alloys, respectively. (D) The melting temperatures and latent heats of fusion of 53 metals and alloys.

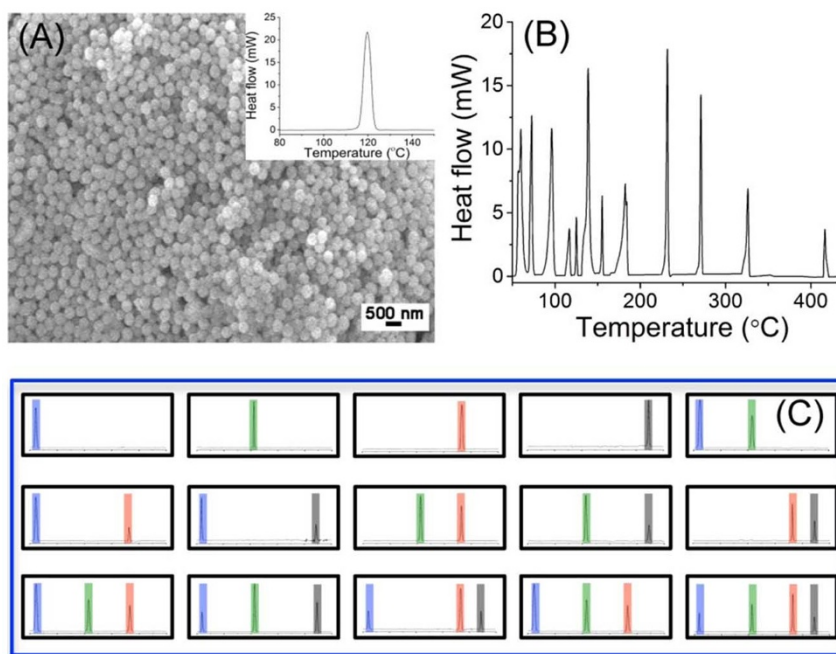


Figure 2 | (A) TEM image and DSC (inset) of silica encapsulated indium-tin nanoparticles. (B) DSC of 12 types of nanoparticles collected from DNT debris. (C) A library of barcodes formed by four types of phase change nanoparticles (indium, tin, bismuth and indium-tin-bismuth eutectic alloy).

solid nanoparticles are then homogeneously mixed with drug powder (i.e., acetaminophen as example) and can either fill capsules, or be compressed at 1 MPa pressure to form tablets. The physical appearance of the drug after adding nanoparticles is indistinguishable from the drug itself to the naked eyes (Figure 3C). In addition, the aqueous suspension of nanoparticles is stable (Figure 3C inset), suggesting the

possibility of using organic solid nanoparticles to authenticate drug in liquid form. The corresponding melting peaks of nanoparticles are observed when the tablet is grounded into powder and tested with DSC (Figure 3D inset). Figure 3D shows a linear relationship existing between the peak area and the mass of nanoparticles loaded in the drug, which is in good agreement with equation (2)

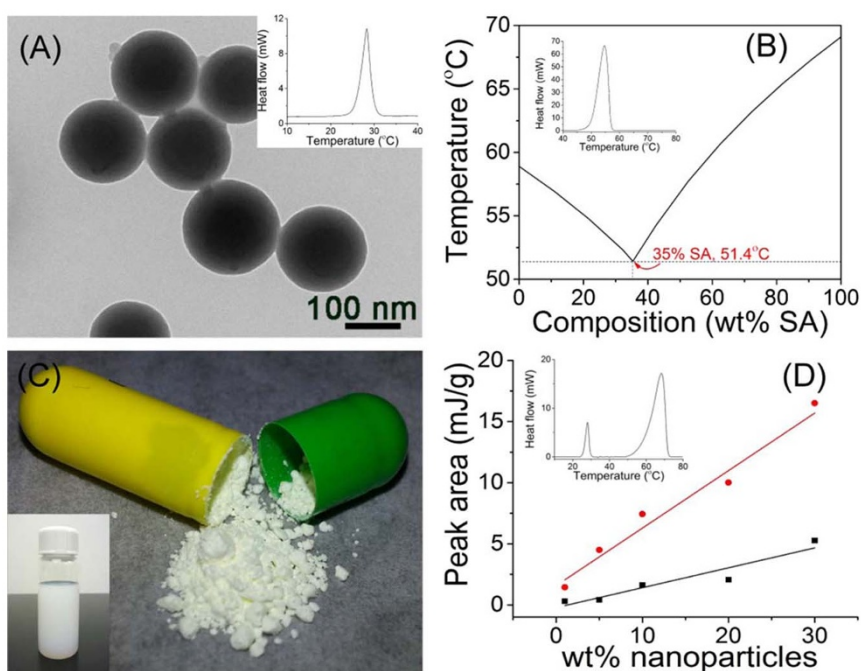


Figure 3 | (A) TEM image and DSC (inset) of polystyrene encapsulated paraffin nanoparticles. (B) Calculated phase diagram of palmitic acid and stearic acid, and the corresponding DSC of their eutectic mixture (inset). (C) Organic solid nanoparticles encoded acetaminophen and an aqueous suspension of encapsulated stearic acid nanoparticles (inset). (D) Peak area calculated from the melting peaks (inset) of stearic acid (circle) and wax (square) nanoparticles at various mass loaded in acetaminophen.

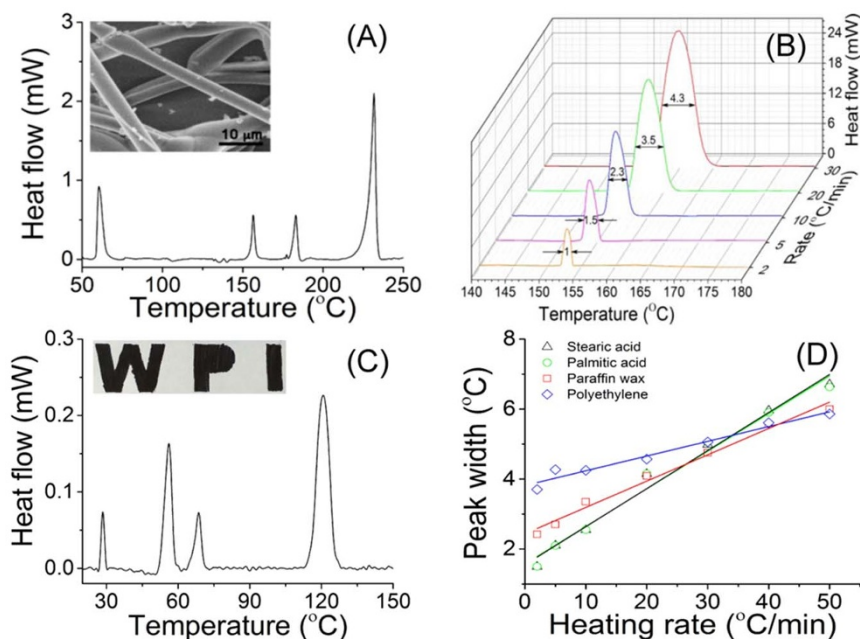


Figure 4 | (A) DSC of four types of nanoparticles contained in microfibers (inset). (B) DSC of indium nanoparticles at different heating rates. (C) DSC of four types of organic solid nanoparticles encoded in painted letters (inset). (D) Peak width of organic solid nanoparticles at different heating rate.

$$Q = m \times C_p \times \beta \quad (2)$$

where Q is the heat flow (melting peak area), m , C_p and β are sample mass, specific heat of sample, and heating rate, respectively. The melting peak area is derived by integrating heat flow over the melting range of the nanoparticles. The lowest detection limit of organic solid nanoparticles is determined to be 1% by weight. The cytotoxicity of organic solid nanoparticles is assessed with MTT assay, where no appreciable toxicity to HeLa cells at 100 μM concentration is found after 10 hour exposure (Figure S3C).

Selected phase change nanoparticles can also be added in polymer and ink, which can be used as covert barcode in textiles and in printing products for anti-counterfeiting purposes. Figure 4A shows the DSC curves of 4 types of nanoparticles in microfibers (inset) formed by ejecting the mixture of poly methylmethacrylate (PMMA), indium, tin, bismuth-indium-tin, and lead-tin nanoparticles. The sensitivity of decoding depends on the mass of the nanoparticles and the minimal heat flow detected by DSC as shown in equation (2). The root-mean-square (RMS) noise of a commercial DSC (PerkinElmer 7) is about 0.02 μW , which corresponds to the lowest detectable mass of ~ 0.05 mg indium/tin at 2°C min^{-1} . For a certain amount of indium nanoparticles (2 mg), the measured heat flux is proportional to the heating rate, meaning the sensitivity can be enhanced by increasing heating rate (Figure 4B). In another sample, four types of organic solid nanoparticles are suspended in ink, which is used to paint the letters “WPI” (Figure 4C inset). The painting is tested with DSC, which confirmed the presence of the four nanoparticles (Figure 4C). Figure 4D shows the relation between the peak width and heating rate of the particles suspended in ink, where the decoding time can be reduced to less than 1 min at a heating rate of $50^\circ\text{C min}^{-1}$ (Figure S4). By operating DSC at a higher heating rate, the signal intensity can be amplified, and detection time can be reduced, though peak width increases as well¹⁸.

A new covert barcode system based on phase change nanoparticles of metallic materials and organic solids has been demonstrated. The nanoparticles are designed using phase diagram knowledge, and have sharp melting peaks and large latent heats of fusions. The method has extremely high labeling capacity owing to small sizes

of nanoparticles, sharp melting peaks and large temperature range of thermal analysis. Selected panels of nanoparticles have been added in explosives, drugs, polymers and ink. This new thermal taggant system will greatly enhance forensic investigation by its technical readiness, structural covertness and robustness.

Methods

Synthesis of metallic nanoparticles. Metal and alloy nanoparticles with eutectic compositions are made by the emulsion process, where metallic powders are boiled in a high boiling point solvent such as poly- α -olefin (PAO) at 180°C for 3 hours under magnetic stirring. After reaction, the solution is centrifuged to remove solvent and thoroughly washed by acetone. Alternately, organometallic precursors are mixed at stoichiometric ratio in micelles, and chemically or thermally reduced to metal atoms, which then aggregate to form metallic nanoparticles. To encapsulate nanoparticles in silica shells, the sol-gel method is used after collecting the nanoparticles from PAO by centrifuging. Tetraethyl-orthosilicate (TEOS) is added in an ethanolic suspension of indium nanoparticles, followed by drop-wise addition of ammonium hydroxide at 60°C . After 90 min, the encapsulated nanoparticles are washed with ethanol.

Synthesis of organic solid nanoparticles. Organic solids are melted in the presence of surfactant at a certain temperature. An aqueous solution containing 2% (volume) of Tween 20 is heated to the same temperature. The molten organic solid is slowly added into the heated aqueous solution while stirring. After 20 minutes, the emulsion is added into 0°C water. The particles are collected by centrifuging at 8000 rpm for 30 minutes, and washed thoroughly with water. To obtain polystyrene encapsulated wax nanoparticles, 10 g of octadecane, 1 g of acrylate acid and 0.1 g of dodecylmercaptan are dissolved in 10 g of styrene by sonication for 10 min. The mixture is poured into 30 g of aqueous solution containing 0.2 g of sodium dodecyl sulfate and 0.2 g of Triton X-100. The entire mixture is then sonicated for 10 min. The flask is purged by nitrogen for 30 minutes, followed by heating at 70°C for 12 hours at 200 rpm to complete polymerization.

1. Yoon, B. *et al.* Recent functional material based approaches to prevent and detect counterfeiting. *J. Mater. Chem. C* **1**, 2388–2403 (2013).
2. Fayazpour, F. *et al.* Digitally encoded drug tablets to combat counterfeiting. *Adv. Mater.* **19**, 3854–3858 (2007).
3. Botti, S. *et al.* Trace level detection and identification of nitro-based explosives by surface-enhanced Raman spectroscopy. *J. Raman Spectrosc.* **44**, 463–468 (2013).
4. Kolla, P. The application of analytical methods to the detection of hidden explosives and explosive devices (vol 36, pg 800, 1997). *Angew. Chem. Int. Ed.* **36**, 1371–1371 (1997).
5. Germain, M. E. & Knapp, M. J. Optical explosives detection: from color changes to fluorescence turn-on. *Chem. Soc. Rev.* **38**, 2543–2555 (2009).
6. MacCrehan, W. A. A NIST Standard Reference Material (SRM) to Support the Detection of Trace Explosives. *Anal. Chem.* **81**, 7189–7196 (2009).



7. Huang, C. B. *et al.* Unbreakable Codes in Electrospun Fibers: Digitally Encoded Polymers to Stop Medicine Counterfeiting. *Adv. Mater.* **22**, 2657–2662 (2010).
8. Braeckmans, K. *et al.* Encoding microcarriers by spatial selective photobleaching. *Nat. Mater.* **2**, 169–173 (2003).
9. Han, S. *et al.* Lithographically Encoded Polymer Microtaggant Using High-Capacity and Error-Correctable QR Code for Anti-Counterfeiting of Drugs. *Adv. Mater.* **24**, 5924–5929 (2012).
10. Clelland, C. T., Risca, V. & Bancroft, C. Hiding messages in DNA microdots. *Nature* **399**, 533–534 (1999).
11. Bera, D., Qian, L., Tseng, T. K. & Holloway, P. H. Quantum Dots and Their Multimodal Applications: A Review. *Mater.* **3**, 2260–2345 (2010).
12. Cao, Y. W. C., Jin, R. C. & Mirkin, C. A. Nanoparticles with Raman spectroscopic fingerprints for DNA and RNA detection. *Science* **297**, 1536–1540 (2002).
13. Nicewarner-Pena, S. R. *et al.* Submicrometer metallic barcodes. *Science* **294**, 137–141 (2001).
14. Jiang, H. J., Moon, K. S., Dong, H., Hua, F. & Wong, C. P. Size-dependent melting properties of tin nanoparticles. *Chem. Phys. Lett.* **429**, 492–496 (2006).
15. Ma, Z. Y., Hong, Y., Zhang, M. H. & Su, M. Encoding and decoding nanoscale thermal barcodes for ultrahigh capacity identification systems. *Appl. Phys. Lett.* **95**, 233101–233101–233103 (2009).
16. Boettinger, W. J., Kattner, U. R., Moon, K.-W. & Perepezko, J. H. DTA and heat-flux DSC measurements of alloy melting and freezing. *NIST Recommended Practice Guide special publication*, 960–915 (2006).
17. Rubin, G. & Finel, A. Calculation of Phase-Diagrams of Ternary-Systems with Cluster-Variation-Method Entropy. *J. Phys.-Condens. Mat.* **5**, 9105–9120 (1993).
18. Vandoreen, A. A. & Muller, B. W. Influence of Experimental-Variables on Curves in Differential Scanning Calorimetry .3. Effects on Peak Height, Peak Width, Shape Index and Baseline Displacement. *Thermochim. Acta* **49**, 175–183 (1981).

Acknowledgments

This project has been supported by a grant from National Institute of Justice (2012-DN-BX-K021) and a grant from National Science Foundation (1055599).

Author contributions

B.D., H.L., L.M., M.S. designed the study; B.D., H.L., conducted the experiment and collected data. B.D. analyzed the results; B.D., H.L., L.M., M.S. discussed the results. B.D., M.S. wrote the manuscript. All authors reviewed the manuscript.

Additional information

Supplementary information accompanies this paper at <http://www.nature.com/scientificreports>

Competing financial interests: The authors declare no competing financial interests.

How to cite this article: Duong, B., Liu, H.L., Ma, L.Y. & Su, M. Covert thermal barcodes based on phase change nanoparticles. *Sci. Rep.* **4**, 5170; DOI:10.1038/srep05170 (2014).



This work is licensed under a Creative Commons Attribution-NonCommercial-ShareAlike 3.0 Unported License. The images in this article are included in the article's Creative Commons license, unless indicated otherwise in the image credit; if the image is not included under the Creative Commons license, users will need to obtain permission from the license holder in order to reproduce the image. To view a copy of this license, visit <http://creativecommons.org/licenses/by-nc-sa/3.0/>